https://doi.org/10.1038/s44407-025-00010-z

Long-term trends of black carbon levels, sources, and radiative effects from 2013 to 2022 in Beijing, China

Yu Xie[1], Linghan Zeng[1], Shuya Hu[1], Tiantian Wang[1], Zhuofei Du[1], Tianyi Tan[1], Nan Xu[1], Shiyi Chen[1], Jianjiong Mao[1], Feng Xu[1] & Min Hu[1,2] ✉

Black carbon (BC), from incomplete combustion of biomass burning and fossil fuels, significantly impacts air pollution and climate. A long-term analysis of BC sources and radiative effects in key regions is essential for the development and refinement of more targeted air quality management strategies. However, there is a lack of sufficient studies addressing this issue. This study examines BC levels and sources from 2013 to 2022. Results show that air quality management measures lowered BC concentrations from 2.23 ± 1.94 μg m^{-3} in 2013 to 0.84 ± 0.71 μg m^{-3} in 2022. The most significant reductions in concentrations occurred during the heating season, which is attributed to the transition from coal-based energy to cleaner-burning gas. Significant reductions in BC were observed from both biomass burning and fossil fuels sources, with average annual reduction rates of 0.06 ± 0.01 μg m^{-3} yr^{-1} and 0.13 ± 0.03 μg m^{-3} yr^{-1}, respectively. BC levels were notably lowest in 2020 and 2021, primarily due to traffic control measures implemented during the COVID-19. This period offers a relevant scenario for examining BC trends under restricted traffic conditions. The relaxation of these measures in 2022 led to a subsequent rise in BC levels. To isolate the pandemic's effect and accurately assess the effectiveness of air quality management measures, the direct radiative effect of BC was calculated for 2013 and 2019, showing a 80% reduction. This research provides essential evidence for understanding the long-term trends of BC in Beijing and its response to previous measures, supporting the development of more effective, targeted BC reduction strategies critical to sustaining long-term improvements in both air quality and climate outcomes.

Beijing, a bustling global metropolis, has achieved an urbanization rate exceeding 87%[1]. Historical economic growth, industrialization, and urbanization models that neglected environmental considerations have led to increased $PM_{2.5}$ (particulate matter with an aerodynamic diameter ≤ 2.5 μm) concentrations[2]. In January 2013, Beijing endured several episodes of severe, persistent haze, adversely affecting human health, causing substantial economic losses, and garnering global attention as the "Airpocalypse"[3,4]. This episode featured alarmingly high $PM_{2.5}$ levels, averaging 231 μg m^{-3} and peaking above 400 μg m^{-3} [5,6]. In response, the government launched the Air Pollution Prevention and Control Action Plan[7] (https://www.gov.cn/zhengce/content/2013-09/13/content_4561.htm, last access: 15 October 2024) in 2013, the Three-Year Action Plan for Winning the Blue Sky Defense Battle[8] (https://www.gov.cn/zhengce/content/2018-07/03/content_5303158.htm, last access: 15 October 2024) in 2018, and the Implementation Plan for Synergizing Reduction of Pollution and Carbon Emission[9] (https://www.mee.gov.cn/xxgk2018/xxgk/xxgk03/202206/t20220617_985879.html, last access: 15 October 2024) in 2022. These initiatives included restructuring the energy sector, stricting vehicle emission standards, phasing out obsolete industrial capacities, and closing high-pollution factories[10,11]. Consequently, Beijing's air quality has improved significantly over the past decade[12,13], with the annual average $PM_{2.5}$ concentration reduced from 89.5 μg m^{-3} in 2013 to 30 μg m^{-3} in 2022, representing a reduction of 67% (https://english.www.gov.cn/news/topnews/202301/04/content_WS63b578d6c6d0a757729e5160.html, last access: 15 October 2024). Furthermore, concentrations of other major pollutants like PM_{10}, SO_2, CO, and NO_2 have also significantly declined due

[1]State Key Laboratory of Regional Environment and Sustainability, International Joint Research Center for Atmospheric Research (IJRC), College of Environmental Sciences and Engineering, Peking University, Beijing, 100871, China. [2]Collaborative Innovation Center of Atmospheric Environment and Equipment Technology, Nanjing University of Information Science & Technology, Nanjing, 210044, China. ✉e-mail: minhu@pku.edu.cn

to structural changes in industry, energy, and transportation[14,15]. Additionally, since the onset of the COVID-19 pandemic in spring 2020, air pollutants have further decreased, enhancing environmental quality[16,17].

Carbonaceous aerosols are the predominant component of ambient $PM_{2.5}$[18,19]. Among them, light-absorbing carbonaceous aerosols play an important role[18,19]. Light-absorbing carbonaceous aerosols mainly consist of black carbon (BC) and brown carbon (BrC)[20]. BC effectively absorbs light across a broad spectral range, from the ultraviolet to the near-infrared spectrum[21], while BrC primarily absorbs ultraviolet light[22]. These particles significantly influence Earth's climate by scattering and absorbing solar radiation, and they can also indirectly modify cloud reflectivity and precipitation processes[23–25]. The radiative heating effect alters air temperature distribution, which reduces the tropospheric boundary layer's height, exacerbating pollutant accumulation near the ground and intensifying haze severity, a phenomenon termed as the "dome effect"[26]. According to the latest IPCC AR6 report[27], the effective radiative forcing of BC ranges from -0.28 to +0.41 W m^{-2}, potentially increasing global temperatures by up to 0.1 °C. BrC's radiative contribution is approximately one-fourth that of BC[28,29]. A substantial portion of BC and BrC emissions is anthropogenic[30], with China playing a significant role in global anthropogenic BC emissions[24,31]. Reducing emissions can control the concentration and impact of these absorbing particles, thus mitigating global warming[32]. In this context, studying the light-absorbing properties of these particles can serve as an indicator of the effectiveness of emission reduction measures[33].

Light absorption-based techniques, which are widely utilized to measure atmospheric light-absorbing particles, offer a more direct assessment of aerosol optical properties and their radiative effects[24,34,35]. Common instruments include the Aethalometer (AE), Multi Angle Absorption Photometer (MAAP), and Photoacoustic Spectroscopy (PAS). Each of these instruments has distinct advantages and limitations[36]. Among them, the AE is commercially available, cost-effective, and easy to operate, enabling simultaneous and continuous measurement of aerosol absorption across multiple wavelengths[35]. Various commonly used methods for BC source apportionment exhibit unique strengths and weaknesses[37]. Notably, while the Aethalometer model relies on assumed parameter values (e.g., absorption Ångström exponents, AAE), which introduce uncertainty in source identification and may not account for all BC sources, it provides high temporal resolution and ease of operation[37,38]. Furthermore, when fixed values are applied, no auxiliary data sources are required. Consequently, this model has been widely adopted in BC source apportionment studies to distinguish between biomass burning (BB) and fossil fuel (FF) sources[38–40]. Studies indicate that in Beijing, the predominant source of BC is FF, particularly during clean days[41,42]. This pattern is similar in other major urban centers such as Guangzhou[43], Shanghai[44], Wuhan[39], and Milan[45], where FF is the dominant source. Conversely, in background atmosphere like the Himalaya[46] and Tibetan Plateau[47], BB and FF contributions are nearly equivalent. However, comprehensive long-term analyses characterizing these sources in Beijing are lacking, and their corresponding radiative effects have not been considered.

In this study, we measured the mass concentration of BC over a ten-year period using an AE at an urban site of the Peking University Urban Atmosphere Environment Monitoring Station (PKUERS). We performed source apportionment with the Aethalometer model, classifying the sources into BB and FF combustion. Based on these classifications, we examined the annual, seasonal, and diurnal variations. Additionally, we employed the Santa Barbara DISORT Atmospheric Radiative Transfer (SBDART) model to calculate the direct radiative effect (DRE) of BC across different seasons and sources. The results enhance our understanding of long-term BC trends in Beijing and its response to previous air pollution control measures and the COVID-19 lockdown, providing important insights for formulating more effective strategies for BC emission reduction.

Results and discussion

Temporal variations of BC

Figure 1 shows the annual variations of BC, $PM_{2.5}$, and BC/$PM_{2.5}$ from 2013 to 2022. It is evident that from 2013 to 2021, the annual average mass concentration of BC exhibited a general declining trend, decreasing from 2.23 ± 1.94 μg m^{-3} to 0.41 ± 0.40 μg m^{-3}, corresponding to a reduction of approximately 82%. The annual mean value for 2021 may be underestimated due to missing winter data. However, the significant decreases observed in the other three seasons, as identified by the Mann-Kendall trend test (Table S1), confirm a consistent declining trend from 2013 to 2021. This declining trend is analogous to the declining BC mass concentration trends in Beijing reported by Xia et al.[48] for the period 2005 to 2017 and Sun et al.[49] for the period 2012 to 2020. Also, the annual mean values of $PM_{2.5}$ and BC/$PM_{2.5}$ exhibited similarly decreasing trends from 2013 to 2021. These decreasing trends indicate a substantial shift in the structure of primary emission sources, attributed to the implementation of the Air Pollution Prevention and Control Action Plan (2013–2017) and the Three-Year Action Plan for Winning the Blue Sky Defense Battle (2018–2020). These measures have been more effective in reducing BC than $PM_{2.5}$, likely because BC primarily originates from primary emissions and is directly controlled by emission reduction policies, whereas $PM_{2.5}$ concentrations are influenced by multiple factors[48]. The annual average BC concentration is lower than that of several urban monitoring sites during the same period, including those in Wuhan[50], Nanjing[51], Baoding[52], and Chiang Mai[53], indicating that Beijing experiences relatively lower BC pollution levels. Besides, comparing the results of this study with those from different background sites during the same period (Table 1), it is evident that the gap between our study and the background sites is gradually narrowing, but our results remain higher. The concentration changes at background sites are relatively minor. For example, the declining trend at Waliguan from 2008 to 2017 was only 2% per year[54], indicating that emission reduction measures have had less impact on these areas compared to urban sites. Additionally, the distribution of BC concentration data points in Beijing is becoming

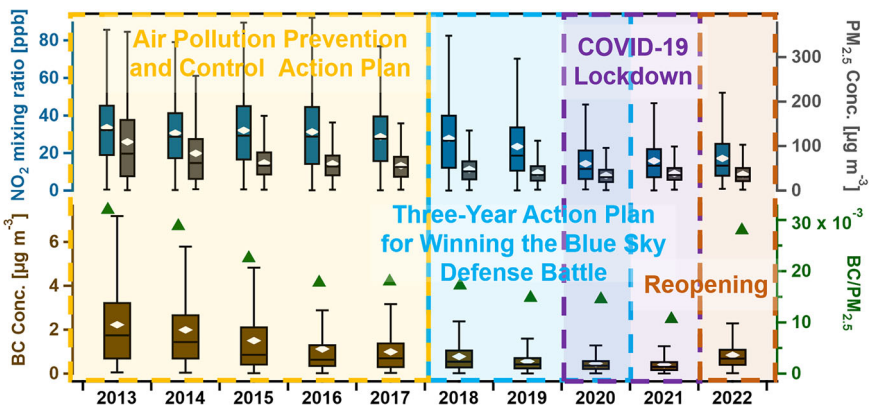

Fig. 1 | Annual variations of BC, $PM_{2.5}$, BC/$PM_{2.5}$, and NO_2. The median (horizontal line), mean (markers), 25th and 75th percentiles (lower and upper box), and 10th and 90th percentiles (lower and upper whiskers) are also shown.

Table 1 | BC concentration [μg m^{-3}] measured in Beijing (BJ, italics) and comparison with different background sites (BG) in China

$Time_{BJ}$	$Time_{BG}$	$Sites_{BG}$	$Conc._{BG}$	$Conc._{BJ}$	$Reference_{BG}$
Jan. 2013–Jun. 2013	Nov. 2012–Jun. 2013	Ranwu	0.14	*1.99 ± 1.62*	111
		Beiluhe	0.41		
2014–2016		Nam Co Lake	0.061	*1.52 ± 1.63*	112
		Mount Qomolangma	0.154		
May 2015–Apr. 2016		Nam Co Lake	0.15 ± 0.85	*1.26 ± 1.41*	113
May 2015–May 2017		Mount Qomolangma	0.30 ± 0.34	*1.17 ± 1.34*	114
Jan. 2016–May 2017, Jan. 2018–Jan. 2019		Mount Qomolangma	0.30 ± 0.33	*0.96 ± 1.05*	46
2017		Waliguan	0.31	*0.99 ± 1.00*	115
Mar. 2018		Mount Qomolangma	0.45 ± 0.56	*1.41 ± 0.87*	116
Jul. 2018–Jun. 2019		Yaze Village	0.18 ± 0.09	*0.67 ± 0.67*	117
Jun. 2019–Jun. 2020		Meili Snow Mountains	0.42 ± 0.37	*0.46 ± 0.38*	118
Sept. 2022–Nov. 2022	Sept. 2022–Dec. 2022	Ordos	0.46	*1.11 ± 0.72*	119

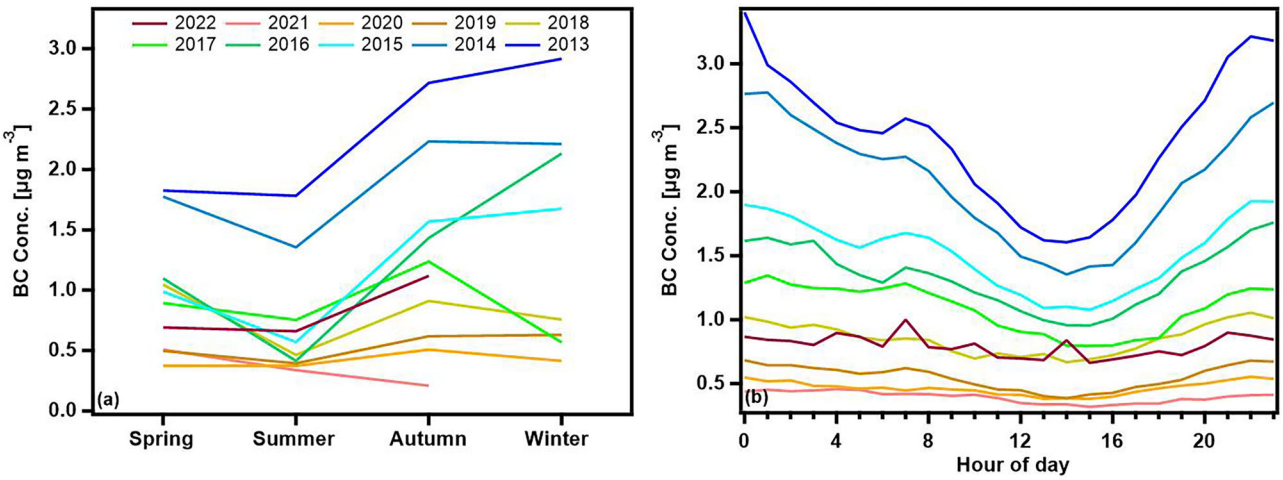

Fig. 2 | Variations in the mass concentration of BC. a Seasonal variations. **b** Diurnal variations.

more concentrated, with annual variations decreasing, suggesting a reduction in extreme pollution events. BC levels were notably lowest in 2020 and 2021, primarily due to traffic control measures implemented during the pandemic. This period offers a relevant scenario for examining BC trends under restricted traffic conditions.

However, in 2022, there was a resurgence in BC levels to 0.84 ± 0.71 μg m^{-3}, approaching the levels observed in 2018, indicating an overall reduction of about 62% from 2013 to 2022. The Mann-Kendall trend test supported that the decrease in BC from 2013 to 2022 was significant (Table S1). The increase of BC concentration in 2022 may be attributed to the relaxation of COVID-19 restrictions, leading to a resurgence of economic activity, especially in transportation, compared to 2021[55–57]. In 2022, the volume mixing ratio of NO_2 at the same site slightly increased (Fig. 1), partially explaining the rebound in BC due to the recovery of traffic activity. Additionally, $PM_{2.5}$ is influenced by more complex factors; for example, the reduction of secondary aerosols may have offset the increase in $PM_{2.5}$ resulting from higher BC concentrations[58], leading to no significant change in $PM_{2.5}$ levels. Similar findings have been reported in other studies on Beijing[58]. Notably, the 2022 data for this site lack winter measurements, suggesting that the actual annual mean value may be even higher. This finding further indicates that BC concentrations could be reduced beyond 2022 levels through enhanced emission control measures. It underscores the necessity of developing effective BC emission reduction strategies, particularly in light of increasing economic activity and traffic emission.

As illustrated in Fig. 2a, the mass concentrations of BC over different years have exhibited a relatively consistent seasonal pattern, characterized by higher levels in winter and lower levels in summer. This seasonal pattern can be attributed to the relatively stable nature of traffic emissions throughout the year, while BB is at its lowest during summer[49]. Additionally, increased precipitation in summer facilitated the removal of pollutants[59]. This pattern is similar to those observed in other urban sites, such as Xi'an[60], Nanjing[61], and Bhubaneswar[62]. Moreover, the mass concentrations of BC decreased ubiquitously during all seasons in 2022 compared to 2013. Excluding the rebound effect observed in 2022, which was attributed to increased post-COVID-19 traffic, reductions in BC concentration across the seasons are more pronounced. From 2013 to 2021, the BC mass concentration decreased by 1.32 μg m^{-3} in spring, 1.44 μg m^{-3} in summer, 2.51 μg m^{-3} in autumn, and 2.50 μg m^{-3} in winter (2013 to 2020). The Mann-Kendall trend test supported that the decrease in BC across all seasons was significant (Table S1). Since 2017, the concentrations have stabilized, showing reduced seasonal variations. Similar seasonal pattern changes have been observed in other studies on Beijing[49,63,64]. This change is primarily due to the significant decrease in BC mass concentration during the autumn and winter seasons (heating season), which has reduced the disparities among the four seasons. From 2013 to 2016, the reduction in BC mass concentration was similar across all four seasons. However, by 2017, the decrease during autumn and winter was nearly double that observed in spring and summer. The implementation of the Clean Winter Heating Plan

for Northern China (2017–2021) has contributed to these decreases (https://www.gov.cn/xinwen/2017-12/21/content_5248986.htm, last access: 15 October 2024). This plan aims to significantly increase the adoption of clean heating systems, with the goal of achieving a substantial transition from coal-based heating to clean heating in smog-affected urbanized areas, including Beijing, within approximately five years. A significant decline was also observed in the spring of 2020, likely due to decreased industrial production and transportation activities associated with COVID-19 pandemic control measures[16,17].

As shown in Fig. 2b, the mass concentration of BC exhibits a pronounced diurnal variation, with higher levels observed in the early morning and at night and lower levels in the afternoon. The minimum concentrations are observed in the afternoon, attributed to the increased mixing layer heights and reduced emissions[65]. The high concentrations observed in the early morning and at night can be explained by a lowering of the boundary layer height and a drop in surface temperature, which create stable temperature inversions during these times[66,67]. Additionally, increased emissions from heavy-duty vehicles and diesel trucks, permitted in the city only between 23:00 and 06:00, contribute to the high concentrations of BC during this period. Especially, prior to 2016, BC levels exhibited distinct elevations during morning rush hours, as depicted in Fig. 2b. After 2016, this diurnal variation weakened and almost disappeared. Additionally, the most notable reductions occurred at night. This can be attributed to several effective policy interventions aimed at controlling air pollution, including removing older vehicles, improving fuel standards, and increasing the use of cleaner energy[12], particularly for diesel vehicles previously restricted to nighttime entry and exit within Beijing. Additionally, the diurnal variations of BC from 2020 to 2021 were much less pronounced, possibly due to a significant reduction in primary emissions, such as those from vehicles, associated with the COVID-19 pandemic[55]. Another contributing factor is that, since November 2019, diesel vehicles compliant with China III emission standards have been prohibited from operating throughout the entire city of Beijing at all times (https://www.beijing.gov.cn/zhengce/zcjd/201905/t20190523_78871.html, last accessed: 15 October 2024).

Optical properties

Figure S1 illustrates the annual variations of $AAE_{370-950}$ and single scattering albedo (SSA_{525}) from 2013 to 2022. AAE quantifies the wavelength dependency of aerosol light absorption. Higher AAE values indicate greater absorption at shorter wavelengths[20]. Over the decade, the lowest annual mean $AAE_{370-950}$ was 1.29 ± 0.18 in 2022, while the highest was 1.42 ± 0.22 in 2015. The $AAE_{370-950}$ in 2022 was lower than in the previous two years, indicating that post-COVID-19 reopening saw greater increases in emissions from high-combustion efficiency sources (e.g., traffic) compared to low-efficiency sources (e.g., BB)[49]. Seasonally, $AAE_{370-950}$ values were higher in winter and lower in summer, reflecting increased BB for heating during the colder months (Fig. S2). Higher SSA values indicate a greater proportion of scattering aerosols. The lowest annual mean SSA_{525} was 0.86 ± 0.07 in 2014, while the highest was 0.95 ± 0.04 in 2021 (Fig. S1). All data were statistically analyzed using the Mann-Whitney U test with Bonferroni correction. Significant differences ($p < 0.05$) were detected across most years and seasons (Tables S2–S4). After 2016, the temporal variation in SSA_{525} became smaller and more stable decreased and stabilized (Mann-Kendall trend test: $p = 0.06$), indicating that the relative proportions of absorbing and scattering components in aerosols became more consistent. The SSA_{525} for 2020 remained consistent with 2019, suggesting that during the COVID-19 lockdown, the reduction in primary emissions (such as light-absorbing particles) was nearly equal to the reduction in scattering, mainly due to secondary aerosols. This finding contrasts with some studies that suggest primary aerosols, including BC and primary organic aerosols, decreased less than secondary aerosols during the pandemic[68,69]. The discrepancy might be due to the fact that those studies focused on the spring of 2020, whereas this study encompasses data from the entire year.

Influence of the local meteorology

Figure S3 presents the bivariate polar plots of BC across four seasons from 2013 to 2022. Annually, the average wind speed (WS) is low, at 2.26 ± 2.03 m s^{-1}. The weak wind conditions significantly contribute to the high air pollution levels in major Chinese cities[70], as low WS promotes the accumulation of pollutants from local sources. Generally, regions with higher BC concentrations correspond to areas with low wind speeds (WS < 3 m s^{-1}). The middle and southern regions show higher BC concentrations, reflecting the combined effects of local emissions and regional transport. During the summer, elevated BC concentrations are primarily observed in a small region close to the sampling site, indicating that local emissions are the primary source[58]. From 2013 to 2017, BC concentrations consistently show higher levels in regions with lower WS, while seasonal variations revealing the different relative influences of regional transport. Since 2018, the southwest has exerted greater influence. The proportion of high wind speeds (WS > 4 m s^{-1}) from the southwest increased from 18% in 2013–2017 to 33% in 2018–2022, while the proportion of high-concentration (BC mass concentration > 0.5 μg m^{-3}) and high-wind-speed events rose from 48% to 67% over the same periods. Over the years, nearly half of the high-concentration BC originated from the southwest. At the PKUERS, the southwest is adjacent to major traffic arteries, including the West Fourth Ring Road and North Fourth Ring Road, likely amplifying the impact of traffic emissions. From the perspective of urban regional transport, this is consistent with previous studies identifying the southwestern region of Beijing's surroundings as a major source of BC pollution[42,71]. The ten-year data indicate that BC concentrations in Beijing are primarily influenced by both local emissions and regional transport, with the influence of regional transport increasing over time.

Sources identified from the Aethalometer model

Sources of BC were apportioned into BB and FF by the method proposed by Sandradewi et al.[38] and Zotter et al.[72] (Fig. S4). For the study period, the mean contributions of FF and BB to total BC were 76% and 24%, respectively. Other studies in Beijing have also indicated that FF combustion is the predominant source of BC[41,42]. This pattern is similar in other major urban centers such as Guangzhou[43], Shanghai[44], the eastern Indo-Gangetic Plain[40], and Milan[45], where FF is the dominant source. However, at background sites such as the Himalayas ($BC_{BB}\%$ > 50%)[46], and the Tibetan Plateau ($BC_{BB}\%$ = 57%)[47], BB and FF contributions are nearly equivalent, with BB sometimes slightly exceeding FF. This difference in the relative proportions of BB and FF partially reflects the disparity between urban and background sites. The annual average concentration of BC_{BB} in Beijing decreased from 0.50 ± 0.60 μg m^{-3} in 2013 to 0.11 ± 0.15 μg m^{-3} in 2022, corresponding to an average annual reduction of 0.06 ± 0.01 μg m^{-3} yr^{-1}. Likewise, BC_{FF} levels declined from 1.73 ± 1.62 μg m^{-3} to 0.74 ± 0.64 μg m^{-3} during the same period, with an average annual decrease of 0.13 ± 0.03 μg m^{-3} yr^{-1}. The BC data from sectoral emissions[73,74] related to BB and FF[75,76] in the Multi-resolution Emission Inventory model for Climate and air pollution research (MEIC) v1.4, with the most recent data updated to 2020 (http://meicmodel.org.cn, last access: 15 October 2024), further supports the source apportionment results ($r = 0.72$). From 2013 to 2020, emissions of BC from both BB and FF-related sectors showed a moderate decline (Figs. S5 and S6). Both BC_{BB} and $BC_{BB\text{-}MEIC}$ exhibited significant seasonal variations, with higher values in cold seasons and lower values in warm seasons. The correlation between BC_{BB} and $BC_{BB\text{-}MEIC}$ ($r = 0.80$, Fig. S5) was higher than that between BC_{FF} and $BC_{FF\text{-}MEIC}$ ($r = 0.62$, Fig. S6), possibly due to greater traffic impact near PKUERS, while MEIC primarily represents coal-dominated emissions across Beijing. Coal was the dominant contributor to FF emissions in Beijing, a trend that was more pronounced in earlier years (accounting for 48% in 2013–2015 but only 6% in 2016–2020). Correspondingly, the difference between BC_{FF} and $BC_{FF\text{-}MEIC}$ was also greater during these periods (Fig. S7b).Additionally, the Aethalometer model used in this study applies fixed classical values to distinguish between FF and BB, which may underestimate FF contributions[77]. Previous studies have also indicated that this method has limitations in analyzing coal sources[40,44],

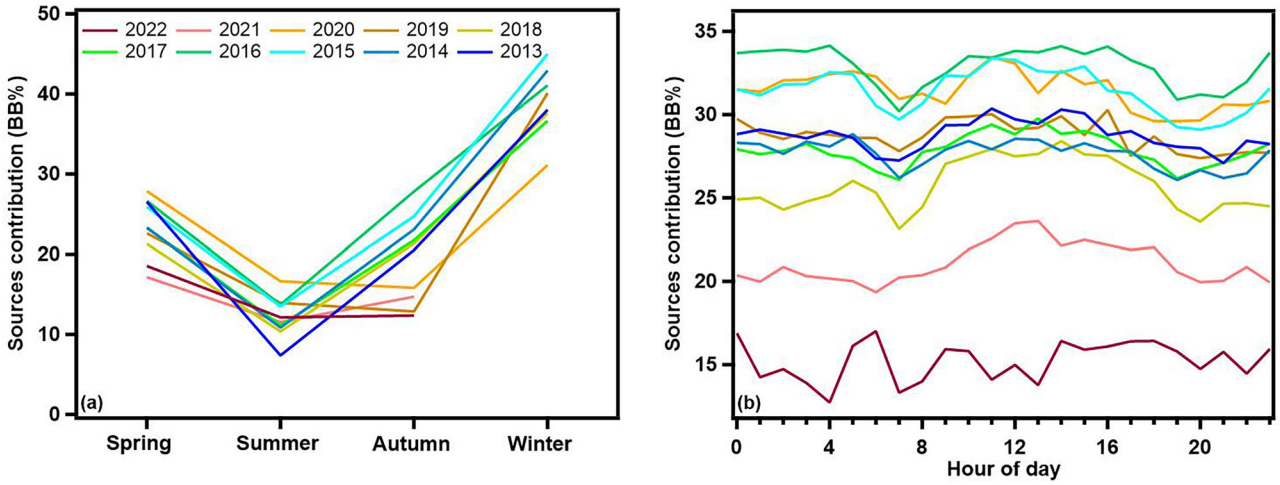

Fig. 3 | Variations in the contribution of biomass burning (BB) combustion to total BC. a Seasonal variations. **b** Diurnal variations.

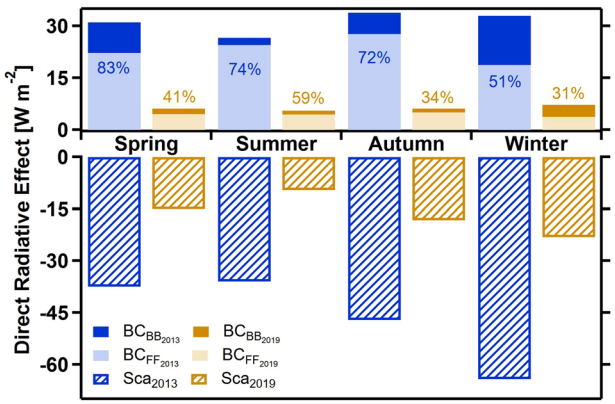

Fig. 4 | Average seasonal atmospheric direct radiative effects (DREs) of absorption (BC_{BB} and BC_{FF}) and scattering at the top of the atmosphere (TOA) for 2013 and 2019. The percentages shown on the BC bar represent the fraction of DRE due to carbonaceous aerosol absorption relative to scattering.

potentially contributing to discrepancies in correlation. The results for BC_{BB} exhibit two plateau periods: 2013–2017 and 2018–2020. The fitting results for both periods are satisfactory, with the first plateau period ($r = 0.89$) being slightly better than the second ($r = 0.83$). However, overall, $BC_{BB\text{-}MEIC}$ during the second plateau period did not align well with the sharp decline observed in BC_{BB}. The discrepancy may result from the measurement being limited to a single monitoring site, whereas the inventory reflects emissions data for the entire city. Overall, controlling BC pollution from traffic sources remains a critical issue, particularly amid the full recovery and rapid expansion of various activities.

Figures 3a and S7a illustrate the seasonal variations of BC_{BB}% and BC_{FF}% from 2013 to 2022, respectively. From 2013 to 2022, the BC_{BB}% (39% ± 5%) in winter was significantly higher than in spring (22% ± 3%), autumn (17% ± 5%), and summer (12% ± 5%). This is primarily due to the cold weather in winter, during which residence BB such as wood, crop remains and straw for heating, resulting in a substantial increase in BB emissions. However, after 2019, a noticeable decline in BC_{BB}% was observed during autumn. The changes after 2019 can be related to the air quality improvement measures implemented by the Chinese government and the COVID-19 pandemic. Overall, the results emphasize the critical importance of reducing BC emissions and controlling FF sources in Beijing. Additionally, during winter months, it is essential to strengthen regulations on BB. The BC_{BB}% and BC_{FF}% diurnal cycles during the different years are displayed in Figs. 3b and S7b. From 2013 to 2020, BC_{FF}% exhibited distinct morning and evening peaks, which were more pronounced than the bimodal pattern of the total BC mass concentration (Fig. 2b), reflecting the diurnal variation of BC emissions from traffic sources. In 2021 and 2022, the diurnal variation became more random, with no clear morning and evening peaks, which may be related to the traffic control measures during the COVID-19 pandemic. However, the overall BC_{FF}% increased significantly compared to previous years, and the mass concentration values slightly rebounded (Fig. S8), which may be related to the gradual relaxation of the COVID-19 control policies and compensatory travel behavior by the public.

Correlation analysis was conducted to further support the identification of BC sources. From 2013 to 2022, the hourly average BC showed significant correlations with CO ($r = 0.83$), and NO_2 ($r = 0.74$), with high correlation coefficients, and it was followed by SO_2 ($r = 0.62$). The correlation coefficients suggesting that BC had similar sources and experienced similar atmospheric processes as these pollutants[78]. Furthermore, NO_2 is widely recognized as a tracer pollutant for vehicle emissions in urban areas[44]. In this study, NO_2 exhibited a higher correlation coefficient with BC than SO_2, suggesting that motor vehicle emissions contributed more significantly to BC concentrations. Tables S5 and S6 present the correlation coefficients between BC_{BB} or BC_{FF} and other air pollutants across different seasons and years, respectively. The correlation between BC_{BB} or BC_{FF} and trace gases, including CO, NO_2, and SO_2, decreases during the summer for several reasons. First, in summer, the concentrations of NO_2 are more influenced by photochemical reactions than by emissions[78], whereas BC concentrations are predominantly influenced by emission sources. Second, increased precipitation in summer enhances the wet deposition of BC[79], contributing to the mass concentration of BC reaching its lowest levels during this season (Fig. 2a). The impact of wet deposition on other gases is comparatively smaller. Overall, BC_{FF} demonstrates a stronger correlation with NO_2 than BC_{BB}. This align with the emission sources of each type of BC and support the results of source apportionment. BC_{BB} exhibits a higher correlation with SO_2 than BC_{FF}, possibly due to higher light absorption at lower wavelengths by aerosols generated from sulfur-containing fuel combustion in Beijing, which may influence the source apportionment model[40].

Direct radiative effects of BC

DRE is a valuable metric for estimating the radiative impacts of various aerosol components[24,80]. Previous research on long-term changes in the DRE in Beijing[49] used forcing equations[81] without accounting for seasonal and source-related variations. In contrast, this study employs the SBDART model, offering a more accurate and reliable approach to radiative forcing studies. Moreover, many prior long-term studies have concentrated exclusively on the effects of BC, overlooking discussions on scattering processes[40,50]. As a result, these studies have inadequately examined changes in the overall radiative properties of aerosols.

A positive DRE indicates net warming, while a negative DRE reflects net cooling[47]. To isolate the influence of the COVID-19 pandemic and more precisely evaluate the effectiveness of governmental air quality management measures, we compare the outcomes from 2013 and 2019. Over this period, the overall aerosol DRE increased from -15.04 W m^{-2} to -10.19 W m^{-2}, suggesting that improvements in air quality have exacerbated climate warming. As illustrated in Fig. 4, while the warming effect of aerosol absorption decreased, the reduction in the cooling effect from scattering was more substantial, underscoring the need for further reductions in light-absorbing aerosols. For BC DRE, the largest reduction occurred in autumn and winter. This finding aligns with the previous observation that the governance effects of BC are more pronounced during the autumn and winter seasons. Overall, the annual average BC DRE value decreased by 80%, from +31.15 W m^{-2} in 2013 to +6.28 W m^{-2} in 2019. The heating effect of light-absorbing particulate matter could offset approximately 70% of the cooling effect induced by scattering particles in 2013. However, following years of mitigation efforts, this offset has decreased, particularly in the winter of 2019, when it was reduced to 31%. This suggests the growing significance of non-light-absorbing particulate matter, which may become a key focus in future air pollution control strategies. Although the radiative impact of light-absorbing particulate matter has been declining, it remains significant, with its offsetting effect on scattering particles still notably higher than the global background level of 1.5% to 1.6%[28]. From a source-based perspective, BC_{BB} contributes more to scattering offset than its share in total BC, indicating its stronger radiative impact. Although BC_{BB} has a lower concentration, its radiative forcing per unit mass is higher. However, BC_{FF} remains the dominant contributor to total DRE, especially in summer. Therefore, for the inherently low concentrations of BC_{BB}, precise regulation of its composition may be more crucial, such as identifying key light-absorbing components. In contrast, controlling BC_{FF} may require a focus on reducing overall emissions.

The absorption properties of BC reduce surface solar radiation, indirectly causing surface cooling, while directly heating the atmosphere, thereby affecting its vertical structure (Fig. S9). Radiative heating by BC affects the air temperature distribution and decreases the tropospheric boundary layer's height. BC and other absorbing aerosols influence the planetary boundary layer (PBL) in large cities through the aerosol-radiation-PBL feedback loop[26]. This change exacerbates the accumulation of pollutants near the surface, increases haze severity, and worsens air pollution. In Beijing, the accumulation of BC may be more pronounced due to weak pressure gradients in the region, which facilitate its buildup within the PBL[82]. Also, the suppression of the boundary layer also confines a significant amount of O_3 precursors below it, which enhances O_3 chemical generation[83]. Nonetheless, the primary effect of BC on O_3 is to reduce the photolysis rate[84], thereby partially decreasing O_3 levels. Numerous studies have demonstrated that BC influences ground-level O_3 concentration by absorbing sunlight and regulating the photolysis rate, the so-called aerosol-photolysis interaction[84–87]. Studies have also shown that the radiative effects of BC may alter the Empirical Kinetics Modeling Approach (EKMA) curve[84]. In Beijing, O_3 concentrations increased in 2019 compared to 2013, while the negative correlation with BC weakened, indicating that BC's contribution to O_3 reduction partially diminished as its radiative effect lessened (Figs. 4 and S10). Therefore, in the context of increased atmospheric oxidizing capacity and aggravated compound pollution, it is imperative to strengthen our focus on the mechanisms of BC-boundary layer interactions and consider formulating targeted measures to address the increasingly complex and comprehensive new air pollution scenarios. Additionally, the radiative effect driven by aerosols could exacerbate the geographic mismatch between national energy supply and demand by reducing solar and wind energy resources[88]. Overall, the radiative effects of BC in Beijing have significantly decreased, but there remains a gap compared to cleaner regions. Developing targeted BC reduction strategies in the future may be more effective, as BC plays a dual role in air pollution and climate change.

Implications and limitations

This study analyzed BC mass concentration in Beijing over a ten-year period, quantifying contributions from BB and FF sources. The results indicate that BC mass concentration decreased from 2.23 ± 1.94 μg m^{-3} in 2013 to 0.84 ± 0.71 μg m^{-3} in 2022, representing a reduction of 62%. This decline reflects the positive impacts of the Air Pollution Prevention and Control Action Plan (2013–2017) and the Three-Year Action Plan for Winning the Blue Sky Defense Battle (2018–2020), particularly the sharp decrease in concentrations during nighttime and in heating season. However, the resurgence of BC levels in 2022 due to increased post-COVID-19 traffic reveals the ongoing challenges in maintaining low pollution levels. Additionally, regional transport from the southwest has exerted greater influence, emphasizing the need for coordinated regional emission control strategies. Source apportionment analysis shows that FF sources dominate BC emissions in Beijing, while BB exhibits a distinct seasonal pattern. Significant reductions in BC were observed from both FF and BB sources, with average annual reduction rates of 0.13 ± 0.03 μg m^{-3} yr^{-1} and 0.06 ± 0.01 μg m^{-3} yr^{-1}, respectively. Additionally, the annual average BC DRE value decreased from +31.15 W m^{-2} in 2013 to +6.28 W m^{-2} in 2019, indicating the broader climate benefits of these air quality interventions. This study aligns with prior research on the long-term trends of BC in Beijing, offering further analyses related to the pandemic and employing the SBDART model for quantitative DRE calculations across different sources and seasons.

However, certain unresolved issues warrant further exploration. For instance, the precision of source apportionment could be improved by incorporating more accurate tracers, such as potassium or levoglucosan. Moreover, the scattering data employed in this study were derived from theoretical equations. Incorporating observational scattering data could improve the precision of radiative calculations. In addition, some emission inventory models may need to account for key policies specific to certain periods to more accurately represent the long-term, non-linear decline in emissions. Overall, the study highlights the necessity for continuous efforts to further reduce BC, especially in light of potential future increases in economic activity and traffic. Effective, targeted BC reduction strategies remain critical to sustaining long-term improvements in both air quality and climate outcomes in Beijing.

Methods

Sampling site

A long-term measurement was conducted at the PKUERS, located on the rooftop of a building on the Peking University campus (39°59′21″ N, 116°18′25″ E), approximately 11 km northwest of Beijing's city center. Further descriptions of this site can be found in earlier publications[59,89,90]. The study covers an observation period from 2013 to 2022. Data gaps, due to the deployment of instruments for other field observations and maintenance, are detailed in Table S7. In this study, the four seasons are defined as follows: spring (March, April, and May), summer (June, July, and August), autumn (September, October, and November), and winter (December, January, and February of the following year).

Instrumentation

Equivalent black carbon (eBC), is derived by converting the light absorption coefficient into mass concentration using a suitable mass absorption efficient. eBC was measured from 2013 to 2022 using a seven-wavelength Aethalometer (AE31, Magee Scientific) at wavelengths of 370, 470, 520, 590, 660, 880, and 950 nm. For simplicity, eBC is referred to as BC. As AE is filter-based, data acquired from it requires careful correction to account for inherent systemic errors, including the filter matrix effect, scattering effect, and loading effect[91,92]. The most important of these is the multiple scattering effect, which was corrected using the method proposed by Weingartner et al.[93]. The raw data (with a 5-minute resolution) obtained from the AE31 was adjusted using the method described by Wu et al.[94] with the Aethalometer Data Processor program in the professional data analysis software IGOR Pro (WaveMetrics inc., Version 6.37). The mass concentration

obtained at 880 nm was used as the measured BC concentration for this study, as BC is the dominant absorber at this wavelength among major aerosol species in the atmosphere[95]. The mass concentration of BC is determined using a mass absorption efficiency of 12.6 $m^2 g^{-1}$ at 880 nm[96]. AAE is calculated[97] by fitting the light absorption coefficient (b_{abs}) to the seven wavelengths, with AAE being the slope of the least-squares fit of the logarithm of b_{abs} (λ) versus the logarithm of these wavelengths[98].

Pollutants including SO_2, NO_2, CO, and O_3, were measured simultaneously using commercial instruments from Thermo Fisher Scientific Inc. (Model 43i-TLE, 42i-TL, 48i-TLE, and 49i). Wind direction and WS were monitored by one automatic meteorological station (Met One Instrument Inc.). The mass concentration of $PM_{2.5}$ was obtained from the air quality monitoring station at Wanliu (39°57′44″ N, 116°17′39″ E; one of the National Control Points), approximately 3 km from our sampling site, provided by the Chinese Ministry of Ecology and Environment (https://www.mee.gov.cn/, last access: 15 October 2024).

Source apportionment

The source apportionment of BC is based on the Aethalometer model from Sandradewi et al.[38]. Here, the BC optical absorption coefficient is assumed to be the sum of BB and FF fractions, with their b_{abs} showing distinct wavelength dependencies characterized by AAE. Absorption coefficients at two wavelengths, 470 nm and 950 nm, were used for source apportionment of total BC as described in Zotter et al.[72]:

$$\frac{b_{abs}(\lambda_1)_{FF}}{b_{abs}(\lambda_2)_{FF}} = \left(\frac{\lambda_1}{\lambda_2}\right)^{-AAE_{FF}} \quad (1)$$

$$\frac{b_{abs}(\lambda_1)_{BB}}{b_{abs}(\lambda_2)_{BB}} = \left(\frac{\lambda_1}{\lambda_2}\right)^{-AAE_{BB}} \quad (2)$$

$$b_{abs}(\lambda_1) = b_{abs}(\lambda_1)_{FF} + b_{abs}(\lambda_1)_{BB} \quad (3)$$

$$b_{abs}(\lambda_2) = b_{abs}(\lambda_2)_{FF} + b_{abs}(\lambda_2)_{BB} \quad (4)$$

According to previous studies, AAE of 0.9–1.1 for FF and 1.8–2.2 for BB have been widely adopted in the Aethalometer model[40]. As lacking synchronous measurement of potassium or levoglucosan to constrain the AAE_{FF} and AAE_{BB}, we chose $AAE_{FF} = 1.0$ and $AAE_{BB} = 2.0$ for source apportionment in this study[39,79,99]. The original Aethalometer model is designed for traffic and biomass burning emissions; however, several confounding factors may affect its accuracy. The presence of secondary organic aerosols (SOA), particularly biogenic SOA, can deposit on the AE31 filter, altering its absorption characteristics. Since biogenic SOA absorption primarily occurs in the ultraviolet region, this interference can be minimized by replacing the 370 nm absorption coefficient with the 470 nm coefficient, as implemented in this study. Another potential confounding factor is the presence of other FF sources, such as coal, despite the absence of coal-fired power plants near the measurement site. Overall, despite these potential sources of interference, the Aethalometer model's assumptions remain valid for this study region, and no specific modifications were made to account for possible biases. Previous studies estimate the uncertainty associated with BC mass concentrations apportioned using the Aethalometer model to be approximately 35–42%[100–102].

Estimations of direct radiative effects

Radiative transfer calculations were performed using the SBDART model[103] to compute the DRE for the wavelength from 250 nm to 4 μm at the top of the atmosphere (TOA). The solar zenith angle is calculated using parameters including longitude, latitude, and UTC time. The surface albedo is 0.15[104]. The aerosol asymmetry factor is 0.65[105]. Aerosol optical parameters at 525 nm were derived from data calculated by Eqs. (5)–(8), including aerosol light scattering coefficient (b_{sca}), SSA, extinction coefficient (b_{ext}), and vertical optical depth of the whole layer aerosols (AOD):

$$b_{sca} = MSE * C \quad (5)$$

$$SSA = \frac{b_{sca}}{b_{sca} + b_{abs}} \quad (6)$$

$$b_{ext} = b_{sca} + b_{abs} \quad (7)$$

$$AOD = \sum_{i=1}^{n} b_{ext} * D_i * F_i \quad (8)$$

where MSE is the mass scattering efficiency, with the value of 5.88 $m^2 g^{-1}$[106] at 525 nm. In the model, the extinction Ångström exponent (EAE) is introduced as 1.12[107] to extrapolate b_{ext} to wavelengths beyond 525 nm (the user-defined reference wavelength). C is the mass concentration of $PM_{2.5}$. D_i and F_i correspond to different depths and the associated cumulative relative fractions of BC, respectively, based on the vertical profile of the relative cumulative fraction measured by Liu et al.[108].

The main outputs of the simulations were downward and upward fluxes at the TOA. The DRE due to scattering ($PM_{2.5}$), denoted as ΔE_{sca}, is defined as the difference between the net solar radiation balance without BC (E_{noBC}, let the $b_{ext} = b_{sca}$, with SSA = 1) and without all aerosols (E_{noaer})[109]. The formulas are as follows:

$$E_{noBC} = E^{\downarrow}_{noBC} - E^{\uparrow}_{noBC} \quad (9)$$

$$E_{noaer} = E^{\downarrow}_{noaer} - E^{\uparrow}_{noaer} \quad (10)$$

$$\Delta E_{sca} = E_{noBC} - E_{noaer} \quad (11)$$

where ↑ and ↓ indicate upward and downward solar radiation, respectively. In a similar manner, the DRE due to absorption (BC), denoted as ΔE_{BC}, can be calculated by Eq. (13)[110]:

$$E_{aer} = E^{\downarrow}_{aer} - E^{\uparrow}_{aer} \quad (12)$$

$$\Delta E_{BC} = E_{aer} - E_{noBC} \quad (13)$$

where E_{aer} is the solar radiation with all aerosols.

When the output layer height is set to the surface, the results at the surface (SUR) can be obtained. Furthermore, the results within the atmosphere (ATM) can be derived using Eq. (14).

$$ATM = TOA - SUR \quad (14)$$

Based on the parameter settings in the Source apportionment section, where $AAE_{FF} = 1.0$ and $AAE_{BB} = 2.0$, the DRE for each source was computed using the SBDART model.

Data availability

Data are available on request from the corresponding author (minhu@pku.edu.cn).

Received: 24 November 2024; Accepted: 18 March 2025;
Published online: 01 May 2025

References

1. Tang, Z. et al. Spatial evolution of urban expansion in the Beijing–Tianjin–Hebei coordinated development region. *Sustainability* **13**, 1579 (2021).
2. Li, G., Fang, C., Wang, S. & Sun, S. The effect of economic growth, urbanization, and industrialization on fine particulate matter (PM 2.5)

concentrations in China. *Environ. Sci. Technol.* **50**, 11452–11459 (2016).
3. Chen, R., Zhao, Z. & Kan, H. Heavy smog and hospital visits in Beijing, China. *Am. J. Respir. Crit. Care Med.* **188**, 1170–1171 (2013).
4. Ferreri, J. M. et al. The January 2013 Beijing "Airpocalypse" and its acute effects on emergency and outpatient visits at a Beijing hospital. *Air Qual. Atmosphere Health* **11**, 301–309 (2018).
5. Sun, Y. et al. Investigation of the sources and evolution processes of severe haze pollution in Beijing in January 2013. *J. Geophys. Res. Atmospheres* **119**, 4380–4398 (2014).
6. Li, S. et al. Satellite and ground observations of severe air pollution episodes in the winter of 2013 in Beijing, China. *Aerosol Air Qual. Res.* **16**, 977–989 (2016).
7. Yu, Y., Dai, C., Wei, Y., Ren, H. & Zhou, J. Air pollution prevention and control action plan substantially reduced PM2.5 concentration in China. *Energy Econ.* **113**, 106206 (2022).
8. Huang, Z., Li, X., Chen, J. & Zhang, D. Does the three-year action plan for winning the Blue Sky Defense Battle implementation enabling the high-quality development of regional energy? A quasi-natural experiment from China. *Energy* **312**, 133405 (2024).
9. Lei, Y. et al. The 2022 report of synergetic roadmap on carbon neutrality and clean air for China: accelerating transition in key sectors. *Environ. Sci. Ecotechnol.***19**, 100335 (2024).
10. Han, X. et al. Seasonal and long-term trends of sulfate, nitrate, and ammonium in PM2.5 in Beijing: implication for air pollution control. *Environ. Sci. Pollut. Res.* **27**, 23730–23741 (2020).
11. Hu, S. et al. Significant changes in the physicochemical properties of BC-containing particles during the cold season in Beijing. *J. Environ. Sci.* **151**, 667–676 (2025).
12. Zhang, Q. et al. Drivers of improved PM2.5 air quality in China from 2013 to 2017. *Proc. Natl. Acad. Sci. USA* **116**, 24463–24469 (2019).
13. Hu, S. et al. Current challenges of improving visibility due to increasing nitrate fraction in PM2.5 during the haze days in Beijing, China. *Environ. Pollut.* **290**, 118032 (2021).
14. Shu, Y. et al. Analysis of the air pollution reduction and climate change mitigation effects of the Three-Year Action Plan for Blue Skies on the "2+26" Cities in China. *J. Environ. Manage.* **317**, 115455 (2022).
15. Chu, F. et al. Air Pollution Characteristics during the 2022 Beijing Winter Olympics. *Int. J. Environ. Res. Public. Health* **19**, 11616 (2022).
16. Marlier, M. E., Xing, J., Zhu, Y. & Wang, S. Impacts of COVID-19 response actions on air quality in China. *Environ. Res. Commun.* **2**, 075003 (2020).
17. Cai, F., Yin, K. & Hao, M. COVID-19 pandemic, air quality, and PM2.5 reduction-induced health benefits: a comparative study for three significant periods in Beijing. *Front. Ecol. Evol.* **10**, 885955 (2022).
18. Zheng, J. et al. Spatial distributions and chemical properties of PM2.5 based on 21 field campaigns at 17 sites in China. *Chemosphere* **159**, 480–487 (2016).
19. Niu, H. et al. Characterization of PM2.5 Carbonaceous Components in a Typical Industrial City in China under Continuous Mitigation Measures. *Toxics* **12**, 461 (2024).
20. Liu, D., He, C., Schwarz, J. P. & Wang, X. Lifecycle of light-absorbing carbonaceous aerosols in the atmosphere. *Npj Clim. Atmospheric Sci.* **3**, 40 (2020).
21. Liu, J. et al. Size-resolved measurements of brown carbon in water and methanol extracts and estimates of their contribution to ambient fine-particle light absorption. *Atmospheric Chem. Phys.* **13**, 12389–12404 (2013).
22. Laskin, A., Laskin, J. & Nizkorodov, S. A. Chemistry of atmospheric brown carbon. *Chem. Rev.* **115**, 4335–4382 (2015).
23. Bond, T. C. & Bergstrom, R. W. Light absorption by carbonaceous particles: an investigative review. *Aerosol Sci. Technol.* **40**, 27–67 (2006).
24. Bond, T. C. et al. Bounding the role of black carbon in the climate system: a scientific assessment. *J. Geophys. Res. Atmospheres* **118**, 5380–5552 (2013).
25. Réveillet, M., et al. Black carbon and dust alter the response of mountain snow cover under climate change. *Nat. Commun.* **13**, 5279 (2022).
26. Ding, A. J. et al. Enhanced haze pollution by black carbon in megacities in China. *Geophys. Res. Lett.* **43**, 2873–2879 (2016).
27. IPCC. *Climate Change 2021: The Physical Science Basis. Contribution of Working Group I to the Sixth Assessment Report of the Intergovernmental Panel on Climate Change*. vol. In Press (Cambridge University Press, Cambridge, United Kingdom and New York, NY, USA, 2021).
28. Zeng, L. et al. Global Measurements of Brown Carbon and Estimated Direct Radiative Effects. *Geophys. Res. Lett.* **47**, e2020GL088747 (2020).
29. Zhang, A. et al. Modeling the global radiative effect of brown carbon: a potentially larger heating source in the tropical free troposphere than black carbon. *Atmospheric Chem. Phys.* **20**, 1901–1920 (2020).
30. Xiong, R. et al. Global brown carbon emissions from combustion sources. *Environ. Sci. Ecotechnology* **12**, 100201 (2022).
31. Ramanathan, V. & Carmichael, G. Global and regional climate changes due to black carbon. *Nat. Geosci.* **1**, 221–227 (2008).
32. Jacobson, M. Z. Strong radiative heating due to the mixing state of black carbon in atmospheric aerosols. *Nature* **409**, 695–697 (2001).
33. Chen, Y. et al. Long-term variation of black carbon and PM2.5 in Beijing, China with respect to meteorological conditions and governmental measures. *Environ. Pollut.* **212**, 269–278 (2016).
34. Sharma, S. et al. Light absorption and thermal measurements of black carbon in different regions of Canada. *J. Geophys. Res. Atmospheres* **107**, (2002).
35. Ran, L., Deng, Z. Z., Wang, P. C. & Xia, X. A. Black carbon and wavelength-dependent aerosol absorption in the North China Plain based on two-year aethalometer measurements. *Atmos. Environ.* **142**, 132–144 (2016).
36. Moosmüller, H., Chakrabarty, R. K. & Arnott, W. P. Aerosol light absorption and its measurement: a review. *J. Quant. Spectrosc. Radiat. Transf.* **110**, 844–878 (2009).
37. Briggs, N. L. & Long, C. M. Critical review of black carbon and elemental carbon source apportionment in Europe and the United States. *Atmos. Environ.* **144**, 409–427 (2016).
38. Sandradewi, J. et al. Using aerosol light absorption measurements for the quantitative determination of wood burning and traffic emission contributions to particulate matter. *Environ. Sci. Technol.* **42**, 3316–3323 (2008).
39. Zheng, H. et al. A 5.5-year observations of black carbon aerosol at a megacity in Central China: Levels, sources, and variation trends. *Atmos. Environ.* **232**, 117581 (2020).
40. Rana, A., Rawat, P. & Sarkar, S. Sources, transport pathways and radiative effects of BC aerosol during 2018–2020 at a receptor site in the eastern Indo-Gangetic Plain. *Atmos. Environ.* **309**, 119900 (2023).
41. Liu, Y., Yan, C. & Zheng, M. Source apportionment of black carbon during winter in Beijing. *Sci. Total Environ.* **618**, 531–541 (2018).
42. Lei, W., Li, X., Yin, Z., Zhang, L. & Zhao, W. Pollution Characteristics and Source Apportionment of Black Carbon Aerosols during Spring in Beijing. *Toxics* **12**, 202 (2024).
43. Zhang, Q. et al. Spatial distribution and sources of winter black carbon and brown carbon in six Chinese megacities. *Sci. Total Environ.* **762**, 143075 (2021).
44. Wei, C. et al. Temporal Characteristics and Potential Sources of Black Carbon in Megacity Shanghai, China. *J. Geophys. Res. Atmospheres* **125**, e2019JD031827 (2020).
45. Mousavi, A. et al. Source apportionment of black carbon (BC) from fossil fuel and biomass burning in metropolitan Milan, Italy. *Atmos. Environ.* **203**, 252–261 (2019).

46. Singh, P. K. et al. Variability of ambient black carbon concentration in the Central Himalaya and its assessment over the Hindu Kush Himalayan region. *Sci. Total Environ.* **858**, 160137 (2023).
47. Liu, H. et al. Measurement report: quantifying source contribution of fossil fuels and biomass-burning black carbon aerosol in the southeastern margin of the Tibetan Plateau. *Atmospheric Chem. Phys.* **21**, 973–987 (2021).
48. Xia, Y. et al. Variation in black carbon concentration and aerosol optical properties in Beijing: Role of emission control and meteorological transport variability. *Chemosphere* **254**, 126849 (2020).
49. Sun, J. et al. Measurement report: Long-term changes in black carbon and aerosol optical properties from 2012 to 2020 in Beijing, China. *Atmospheric Chem. Phys.* **22**, 561–575 (2022).
50. Ma, Y. et al. Black Carbon over Wuhan, China: Seasonal Variations in Its Optical Properties, Radiative Forcing and Contribution to Atmospheric Aerosols. *Remote Sens.* **13**, 3620 (2021).
51. Pei, Y. et al. Analysis of BC Pollution Characteristics under PM2.5 and O3 Pollution Conditions in Nanjing from 2015 to 2020. *Atmosphere* **13**, 1440 (2022).
52. Yang, Z. et al. Characteristics and source apportionment of black carbon aerosol in the North China Plain. *Atmospheric Res.* **276**, 106246 (2022).
53. Pani, S. K. et al. Black carbon over an urban atmosphere in northern peninsular Southeast Asia: Characteristics, source apportionment, and associated health risks. *Environ. Pollut.* **259**, 113871 (2020).
54. Dai, M. et al. Long-Term Variation and Source Apportionment of Black Carbon at Mt. Waliguan, China. *J. Geophys. Res. Atmospheres* **126**, e2021JD035273 (2021).
55. Bakola, M., Hernandez Carballo, I., Jelastopulu, E. & Stuckler, D. The impact of COVID-19 lockdown on air pollution in Europe and North America: a systematic review. *Eur. J. Public Health* **32**, 962–968 (2022).
56. Saha, L. et al. The impact of the COVID-19 lockdown on global air quality: A review. *Environ. Sustain.* **5**, 5–23 (2022).
57. Addas, A. & Maghrabi, A. The Impact of COVID-19 lockdowns on air quality—a global review. *Sustainability* **13**, 10212 (2021).
58. Li, J. et al. Key drivers of the oxidative potential of PM2.5 in Beijing in the context of air quality improvement from 2018 to 2022. *Environ. Int.* **187**, 108724 (2024).
59. Wang, T. et al. Measurement of aerosol optical properties and their potential source origin in urban Beijing from 2013-2017. *Atmos. Environ.* **206**, 293–302 (2019).
60. Zhao, S. et al. Seasonal variation and four-year trend of black carbon in the Mid-west China: The analysis of the ambient measurement and WRF-Chem modeling. *Atmos. Environ.* **123**, 430–439 (2015).
61. Yang, Y. et al. Seasonal size distribution and mixing state of black carbon aerosols in a polluted urban environment of the Yangtze River Delta region, China. *Sci. Total Environ.* **654**, 300–310 (2019).
62. Kompalli, S. K. et al. Seasonal contrast in size distributions and mixing state of black carbon and its association with PM 1.0 chemical composition from the eastern coast of India. *Atmospheric Chem. Phys.* **20**, 3965–3985 (2020).
63. Wu, Y. et al. Effect of source variation on the size and mixing state of black carbon aerosol in urban Beijing from 2013 to 2019: Implication on light absorption. *Environ. Pollut.* **270**, 116089 (2021).
64. Zhang, J. et al. The pollution characterization of black carbon aerosols in the southwest suburb of beijing from 2013 to 2019. *Atmospheric Pollut. Res.* **14**, 101669 (2023).
65. Xie, C. et al. Vertical characterization of aerosol optical properties and brown carbon in winter in urban Beijing, China. *Atmospheric Chem. Phys.* **19**, 165–179 (2019).
66. Wang, H. et al. Determination and climatology of the diurnal cycle of the atmospheric mixing layer height over Beijing 2013–2018: lidar measurements and implications for air pollution. *Atmospheric Chem. Phys.* **20**, 8839–8854 (2020).
67. Mues, A. et al. WRF and WRF-Chem v3.5.1 simulations of meteorology and black carbon concentrations in the Kathmandu Valley. *Geosci. Model Dev.* **11**, 2067–2091 (2018).
68. Sun, Y. et al. A chemical cocktail during the COVID-19 outbreak in Beijing, China: Insights from six-year aerosol particle composition measurements during the Chinese New Year holiday. *Sci. Total Environ.* **742**, 140739 (2020).
69. Li, Z. et al. Nitrate and secondary organic aerosol dominated particle light extinction in Beijing due to clean air action. *Atmos. Environ.* **269**, 118833 (2022).
70. Cao, J. et al. On the potential high acid deposition in northeastern China. *J. Geophys. Res. Atmospheres* **118**, 4834–4846 (2013).
71. Wang, L. et al. Hourly variation characteristics of PM2.5 and main components in Beijing based on wind direction. *Atmos. Environ.* **327**, 120493 (2024).
72. Zotter, P. et al. Evaluation of the absorption Ångström exponents for traffic and wood burning in the Aethalometer-based source apportionment using radiocarbon measurements of ambient aerosol. *Atmospheric Chem. Phys.* **17**, 4229–4249 (2017).
73. Zheng, B. et al. Trends in China's anthropogenic emissions since 2010 as the consequence of clean air actions. *Atmospheric Chem. Phys.* **18**, 14095–14111 (2018).
74. Li, M. et al. Anthropogenic emission inventories in China: a review. *Natl. Sci. Rev.* **4**, 834–866 (2017).
75. Zheng, B. et al. High-resolution mapping of vehicle emissions in China in 2008. *Atmospheric Chem. Phys.* **14**, 9787–9805 (2014).
76. Peng, L. et al. Underreported coal in statistics: A survey-based solid fuel consumption and emission inventory for the rural residential sector in China. *Appl. Energy* **235**, 1169–1182 (2019).
77. Zheng, H. et al. A method to dynamically constrain black carbon aerosol sources with online monitored potassium. *Npj Clim. Atmospheric Sci.* **4**, 43 (2021).
78. Wang, Y. et al. Black carbon and its correlation with trace gases at a rural site in Beijing: Top-down constraints from ambient measurements on bottom-up emissions: BC AND CO CORRELATION NEAR BEIJING. *J. Geophys. Res. Atmospheres* **116**, n/a–n/a (2011).
79. Jing, A. et al. Source apportionment of black carbon in different seasons in the northern suburb of Nanjing, China. *Atmos. Environ.* **201**, 190–200 (2019).
80. Zeb, B. et al. Black Carbon aerosol characteristics and radiative forcing over the high altitude glacier region of Himalaya-Karakorum-Hindukush. *Atmos. Environ.* **238**, 117711 (2020).
81. Chen, Y. & Bond, T. C. Light absorption by organic carbon from wood combustion. *Atmos. Chem. Phys.* (2010).
82. Han, X. & Zhang, M. -G. Assessment of the regional source contributions to PM 2.5 mass concentration in Beijing. *Atmospheric Ocean. Sci. Lett.* **11**, 143–149 (2018).
83. Gao, J. et al. Effects of black carbon and boundary layer interaction on surface ozone in Nanjing, China. *Atmospheric Chem. Phys.* **18**, 7081–7094 (2018).
84. An, J. et al. Analysis of the Effect of Optical Properties of Black Carbon on Ozone in an Urban Environment at the Yangtze River Delta, China. *Adv. Atmospheric Sci.* **38**, 1153–1164 (2021).
85. Latha, K. M. & Badarinath, K. V. S. Correlation between black carbon aerosols, carbon monoxide and tropospheric ozone over a tropical urban site. *Atmospheric Res.* **71**, 265–274 (2004).
86. Li, G., Zhang, R., Fan, J. & Tie, X. Impacts of black carbon aerosol on photolysis and ozone. *J. Geophys. Res. Atmospheres* **110**, 2005JD005898 (2005).
87. Li, J. & Li, Y. Ozone deterioration over North China plain caused by light absorption of black carbon and organic carbon. *Atmos. Environ.* **313**, 120048 (2023).

88. Qin, Y. et al. Amplified positive effects on air quality, health, and renewable energy under China's carbon neutral target. *Nat. Geosci.* **17**, 411–418 (2024).
89. Guo, S. et al. Elucidating severe urban haze formation in China. *Proc. Natl. Acad. Sci. USA* **111**, 17373–17378 (2014).
90. Shang, D. et al. New Particle Formation Occurrence in the Urban Atmosphere of Beijing During 2013–2020. *J. Geophys. Res. Atmospheres* **128**, e2022JD038334 (2023).
91. Bond, T. C., Anderson, T. L. & Campbell, D. Calibration and Intercomparison of Filter-Based Measurements of Visible Light Absorption by Aerosols. *Aerosol Sci. Technol.* **30**, 582–600 (1999).
92. Park, K. et al. Comparison of Continuous and Filter-Based Carbon Measurements at the Fresno Supersite. *J. Air Waste Manag. Assoc.* **56**, 474–491 (2006).
93. Weingartner, E. et al. Absorption of light by soot particles: determination of the absorption coefficient by means of aethalometers. *J. Aerosol Sci.* **34**, 1445–1463 (2003).
94. Wu, C., Wu, D. & Yu, J. Z. Quantifying black carbon light absorption enhancement with a novel statistical approach. *Atmospheric Chem. Phys.* **18**, 289–309 (2018).
95. Bansal, O., Singh, A. & Singh, D. Aerosol Characteristics over the Northwestern Indo-Gangetic Plain: Clear-Sky Radiative Forcing of Composite and Black Carbon Aerosol. *Aerosol Air Qual. Res.* **19**, 5–14 (2019).
96. Hansen, A. D. A. The Aethalometer. Magee Scientific Company, Berkeley, CA (2005).
97. Bergstrom, R. W. et al. Spectral absorption properties of atmospheric aerosols. *Atmos Chem Phys* (2007).
98. Zhang, G. et al. An Improved Absorption Ångström Exponent (AAE)-Based Method for Evaluating the Contribution of Light Absorption from Brown Carbon with a High-Time Resolution. *Aerosol Air Qual. Res.* **19**, 15–24 (2019).
99. Liu, Y. et al. Impacts of COVID-19 on Black Carbon in Two Representative Regions in China: Insights Based on Online Measurement in Beijing and Tibet. *Geophys. Res. Lett.* **48**, e2021GL092770 (2021).
100. Healy, R. M. et al. Ambient measurements and source apportionment of fossil fuel and biomass burning black carbon in Ontario. *Atmos. Environ.* **161**, 34–47 (2017).
101. Martinsson, J. et al. Carbonaceous aerosol source apportionment using the Aethalometer model – evaluation by radiocarbon and levoglucosan analysis at a rural background site in southern Sweden. *Atmospheric Chem. Phys.* **17**, 4265–4281 (2017).
102. Healy, R. M. et al. Black carbon in the Lower Fraser Valley, British Columbia: Impact of 2017 wildfires on local air quality and aerosol optical properties. *Atmos. Environ.* **217**, 116976 (2019).
103. Ricchiazzi, P., Yang, S., Gautier, C. & Sowle, D. SBDART: A Research and Teaching Software Tool for Plane-Parallel Radiative Transfer in the Earth's Atmosphere. *Bull. Am. Meteorol. Soc.* **79**, 2101–2114 (1998).
104. Oke, T. R. *Boundary Layer Climates*. (Methuen, London, 1987).
105. Andrews, E. et al. Comparison of methods for deriving aerosol asymmetry parameter. *J. Geophys. Res. Atmospheres* **111**, (2006), 2004JD005734.
106. Zhao, X., Zhang, X., Pu, W., Meng, W. & Xu, X. Scattering properties of the atmospheric aerosol in Beijing, China. *Atmospheric Res.* **101**, 799–808 (2011).
107. Che, H. et al. Spatial distribution of aerosol microphysical and optical properties and direct radiative effect from the China Aerosol Remote Sensing Network. *Atmospheric Chem. Phys.* **19**, 11843–11864 (2019).
108. Liu, J. et al. Brown carbon aerosol in the North American continental troposphere: sources, abundance, and radiative forcing. *Atmospheric Chem. Phys.* **15**, 7841–7858 (2015).
109. García, O. E. et al. Shortwave radiative forcing and efficiency of key aerosol types using AERONET data. *Atmospheric Chem. Phys.* **12**, 5129–5145 (2012).
110. Zhang, M., Fan, R., Ma, Y., Gong, W. & Shi, Y. Atmospheric aerosol and black carbon optical properties and associated radiative forcing under haze conditions. *J. Quant. Spectrosc. Radiat. Transf.* **259**, 107390 (2021).
111. Wang, M. et al. Two distinct patterns of seasonal variation of airborne black carbon over Tibetan Plateau. *Sci. Total Environ.* **573**, 1041–1052 (2016).
112. Li, C. et al. Re-evaluating black carbon in the Himalayas and the Tibetan Plateau: concentrations and deposition. *Atmospheric Chem. Phys.* **17**, 11899–11912 (2017).
113. Wang, F. et al. Black Carbon: The Concentration and Sources Study at the Nam Co Lake, the Tibetan Plateau from 2015 to 2016. *Atmosphere* **11**, 624 (2020).
114. Chen, X., Kang, S., Cong, Z., Yang, J. & Ma, Y. Concentration, temporal variation, and sources of black carbon in the Mt. Everest region retrieved by real-time observation and simulation. *Atmospheric Chem. Phys.* **18**, 12859–12875 (2018).
115. Guo, B. et al. Long-term variation of black carbon aerosol in China based on revised aethalometer monitoring data. *Atmosphere* **11**, 684 (2020).
116. Xiang, Y. et al. Vertical profile of aerosols in the Himalayas revealed by lidar: New insights into their seasonal/diurnal patterns, sources, and transport. *Environ. Pollut.* **285**, 117686 (2021).
117. Zhang, C. et al. Light absorption and fluorescence characteristics of water-soluble organic compounds in carbonaceous particles at a typical remote site in the southeastern Himalayas and Tibetan Plateau. *Environ. Pollut.* **272**, 116000 (2021).
118. Chen, P. et al. South and Southeast Asia controls black carbon characteristics of Meili Snow Mountains in southeast Tibetan Plateau. *Sci. Total Environ.* **927**, 172262 (2024).
119. Li, Y., Zhang, J., Duan, Q., Kong, X. & Wang, H. Temporal evolution and source apportionment of BC aerosols during autumn in the grassland of Ordos, China. *Meteorol. Appl.* **31**, e2172 (2024).

Acknowledgements

This study was financially supported by the National Natural Science Foundation of China-Creative Research Group Fund (22221004), the National Key Research and Development Program of China (2022YFC3701000, task 1 and 4).

Author contributions

Y.X., L.Z., and M.H. designed the study. Y.X., L.Z., S.H., T.W., Z.D., T.T., N.X., S.C., J.M., and F.X. collected and analyzed the data used in this study. Y.X. wrote the manuscript. All authors reviewed and commented on the manuscript.

Competing interests

Author M.H. serves as Editors-in-Chief of this journal and had no role in the peer-review or decision to publish this manuscript.

Additional information

Supplementary information The online version contains supplementary material available at https://doi.org/10.1038/s44407-025-00010-z.

Correspondence and requests for materials should be addressed to Min Hu.